Structure
Article

Structure of Mega-Hemocyanin Reveals Protein Origami in Snails

Christos Gatsogiannis,[1,2,*] Oliver Hofnagel,[1] Jürgen Markl,[3] and Stefan Raunser[1,2,*]
[1]Department of Structural Biochemistry, Max Planck Institute of Molecular Physiology, Otto-Hahn-Strasse 11, 44227 Dortmund, Germany
[2]Institute of Chemistry and Biochemistry, Freie Universität Berlin, Thielallee 63, 14195 Berlin, Germany
[3]Institute of Zoology, Johannes Gutenberg University, Johannes-von-Müller-Weg 6, 55128 Mainz, Germany
*Correspondence: christos.gatsogiannis@mpi-dortmund.mpg.de (C.G.), stefan.raunser@mpi-dortmund.mpg.de (S.R.)
http://dx.doi.org/10.1016/j.str.2014.10.013

SUMMARY

Mega-hemocyanin is a 13.5 MDa oxygen transporter found in the hemolymph of some snails. Similar to typical gastropod hemocyanins, it is composed of 400 kDa building blocks but has additional 550 kDa subunits. Together, they form a large, completely filled cylinder. The structural basis for this highly complex protein packing is not known so far. Here, we report the electron cryomicroscopy (cryo-EM) structure of mega-hemocyanin complexes from two different snail species. The structures reveal that mega-hemocyanin is composed of flexible building blocks that differ in their conformation, but not in their primary structure. Like a protein origami, these flexible blocks are optimally packed, implementing different local symmetries and pseudosymmetries. A comparison between the two structures suggests a surprisingly simple evolutionary mechanism leading to these large oxygen transporters.

INTRODUCTION

Animals have a continuous need for oxygen to sustain an efficient aerobic metabolism and produce sufficient amounts of ATP. In most mollusks, the crucial role of oxygen transport in the hemolymph is facilitated by the blue respiratory pigment hemocyanin (Decker et al., 2007; van Holde et al., 2001). Evolution, structure, and function of molluscan hemocyanins have been intensively studied during the last decades (Bergmann et al., 2006; Lieb and Markl, 2004; Lieb et al., 2001; Markl, 2013; Miller et al., 1998; Morse et al., 1986), and especially hemocyanins from gastropods, i.e., snails and slugs, have received particular interest because of their remarkable immunological properties in laboratory animals and man (Slovin et al., 2005). A prominent example is keyhole limpet hemocyanin (KLH), which is widely used in medical research and clinical studies as vaccine carrier and as immunotherapeutical agent for the treatment of bladder carcinomas (Becker et al., 2014; Harris and Markl, 1999, 2000). Gastropod hemocyanins are freely dissolved in the blood of the animals and function as large, cylindrical didecamers or even bigger tube-like multidecamers, which are built from 400 kDa subunits. Each subunit is formed by a single polypeptide chain and consists of eight paralogous functional units (FU) (termed FU-a–FU-h) that are connected by short linkers. Each FU carries an oxygen-binding site formed by a pair of copper ions (van Holde et al., 2001) and up to three binding sites for carbohydrate chains (Kurokawa et al., 2002; Lieb et al., 2004; Velkova et al., 2011). Crystal structures of FUs from different molluscan hemocyanins are known (Cuff et al., 1998; Jaenicke et al., 2010, 2011; Perbandt et al., 2003), and electron cryomicroscopy (cryo-EM) in combination with X-ray crystallography revealed the basic overall architecture of the gastropod hemocyanin (didecamer; 8 MDa; Gatsogiannis and Markl, 2009; Lieb et al., 2010; Zhang et al., 2013).

Recently, an unusual gastropod hemocyanin tridecamer was found in fresh/brackish-water cerithioid snails, termed mega-hemocyanin (Lieb et al., 2010). With a molecular mass of 13.5 MDa, mega-hemocyanins are among the largest known oxygen transporters. Its respiratory plasticity exceeds that of usual molluscan hemocyanins and multimeric hemoglobins (Lieb et al., 2010). Therefore, these snails can live under normoxic conditions but can also survive in hypoxic waters. This probably explains the success of members of this taxon in occupying hostile habitats (Lieb et al., 2010). In contrast to common hemocyanins, mega-hemocyanins consist of two different subunits: the typical 400 kDa subunit and an additional subunit of 550 kDa, which represents one of the largest single polypeptides ever reported. The recent analysis of mega-hemocyanins from different cerithioids revealed that the whole complex consists of two canonical decamers that flank an unusual central "mega-decamer," resulting in a hetero-30-mer (Lieb et al., 2010). Twenty copies of the typical 400 kDa subunit form the two peripheral decamers, whereas ten copies of the 550 kDa subunit form the central mega-decamer. The N′-terminal segment a-b-c-d-e-f found in the 400 kDa subunit is also present in the 550 kDa subunit and constitutes the cylinder wall of the central mega-decamer. The two terminal FUs (-g-h) of the 400 kDa subunit, however, have been replaced by six sequential variations of FU-f (termed -f1-f2-f3-f4-f5-f6; Markl, 2013), which completely fill the interior of the hetero-30-meric cylinder. However, the resolution of our previous cryo-EM structure was not sufficient to reveal the exact architecture of the *Leptoxis carinata* mega-hemocyanin (Lieb et al., 2010). Therefore, the structural basis for this highly complex protein packing remained obscure.

Here, we report the complete molecular models of mega-hemocyanins from two different species *Melanoides tuberculata* and *Terebralia palustris*, belonging to two different cerithioid families. The present study reveals a highly complicated origami-like

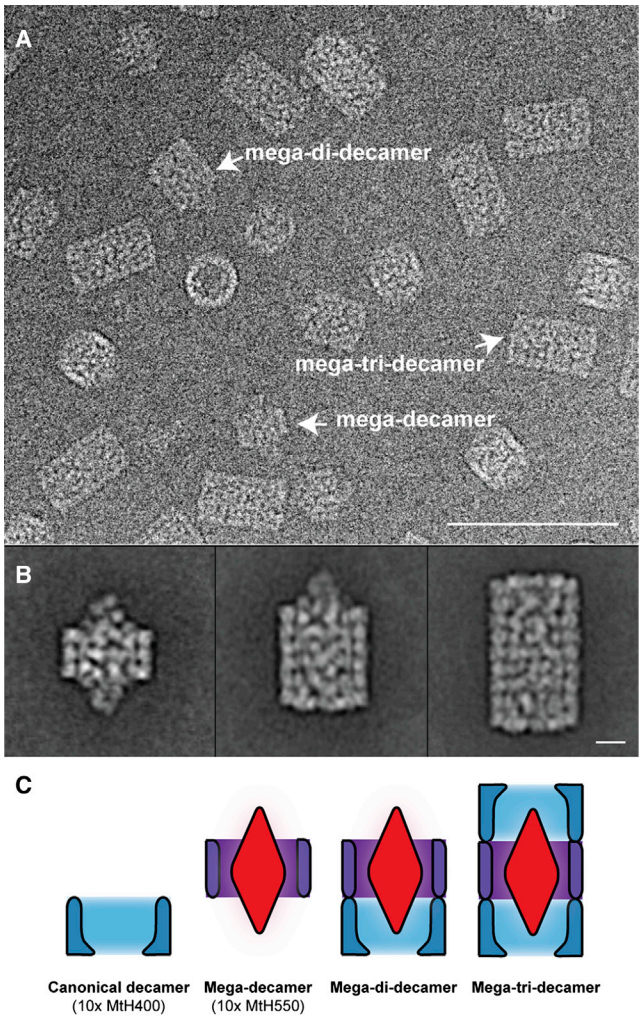

Figure 1. Cryoelectron Microscopy and General Architecture of MtH

(A and B) Subarea of an unprocessed digital micrograph of vitrified MtH, showing mega-decamers (10× MtH550), didecamers (10× MtH400 + 10× MtH550), and hetero-30-mers (10× MtH400 + 10× MtH550 + 10× MtMH400; scale bar: 20 nm; A) and corresponding class averages (B), scale bar: 10 nm. (C) Schematic representation of the general architecture of MtH. Subunit MtH400 forms a typical gastropod hemocyanin decamer (blue), whereas MtH550 forms the mega-decamer, with a typical gastropod hemocyanin cylinder wall (magenta) and an enlarged rhombus-like inner complex (red). The didecamer is a heterodimer of a typical decamer and a mega-decamer, whereas the hetero-30-mer consists of two typical decamers, flanking a central mega-decamer. Note that isolated typical gastropod hemocyanin decamers (blue) are not present in the hemolymph.

packing of the mega-hemocyanin subunits and gives hints about the evolutionary mechanism leading to these large protein complexes.

RESULTS

Cryo-EM Structure of *Melanoides tuberculata* Mega-hemocyanin

We purified mega-hemocyanin from the hemolymph of the highly invasive parasite carrier *Melanoides tuberculata* (MtH) and analyzed it by cryo-EM. In agreement with earlier data (Lieb et al., 2010), a mixture of MtH oligomers (20% mega-decamers, 30% hetero-20-mers, and 50% hetero-30-mers) was present in the sample (Figure 1), making top views, that is axial views, of different complexes indistinguishable. We therefore used only side views of the complete MtH tridecamers (MtH400 decamer + MtH550 mega-decamer + MtH400 decamer) for the reconstruction (Figure 1). Because all hemocyanins structurally characterized so far are 5-fold symmetrical (Gatsogiannis and Markl, 2009; Gatsogiannis et al., 2007; Meissner et al., 2000; Zhang et al., 2013), we routinely applied C5 symmetry during the reconstruction of the MtH tridecamer. Although the FUs in the outer cylinder were nicely resolved and some α helices were visible in form of rod-like densities (Figure S1A available online), the resolution of the rhombus-shaped cylinder core was much lower and most FUs were not discernible (Figure S1B).

2D class averages of mega-decamers showed strong and clear densities in this part of the complex (Figure 1B), ruling out structural flexibility or heterogeneity as possible reasons for the low resolution. We therefore suspected that the core of the mega-decamer is not, like the rest of the complex, 5-fold symmetrical and calculated a reconstruction without imposing symmetry. This time the 60 individual FUs of the mega-decamer core were clearly discernible and showed a 2-fold symmetrical arrangement (Figure S1C). In contrast, the cylinder wall of the central mega-decamer indicated an overall D5 symmetry. Mismatch of symmetry, though unusual, has been observed previously in multicomponent complexes (Beuron et al., 1998; Lander et al., 2012; Lasker et al., 2012; Marles-Wright et al., 2008; Wolf et al., 2010). However, the mega-decamer is the rare case of symmetry mismatch within a homo-oligomeric protein complex.

To take advantage of the 2-fold symmetry of the inner rhombus and D5 symmetry of the outer cylinder, we modified the 3D projection refinement procedure and locally symmetrized the 3D reconstructions. Thus, we obtained a cryo-EM structure of the MtH tridecamer with an average resolution of 12 Å (Figures 2A–2C, S2A, and S2B). Local resolution calculations delineated the cylinder of the central mega-decamer as better resolved (average resolution 9.2 Å) than the cylinder core (average resolution 13.3 Å). The characteristic overall bottle-like appearance of single FUs allowed unambiguous fitting of homology models into their respective density, enabling us to clarify the topology of all 120 FUs of the MtH mega-decamer and thus obtain a complete pseudoatomic model of an entire mega-hemocyanin (Figure S3).

At the resolution of 9.2 Å, the two identical MtH400 decamers flanking the MtH550 mega-decamer (Figure 2) are almost indistinguishable from the decamer of KLH1, which represents the gastropod hemocyanin prototype (Gatsogiannis and Markl, 2009; Figure S4). This suggests that MtH and KLH1 use a similar pathway to transfer forces between adjacent FUs during cooperative oxygen binding. As for all other studied molluscan hemocyanins, the FUs of the MtH400 decamers are arranged as hetero- or homodimers termed "morphological units" (a↔b, c↔f, d↔e, g↔g, and h↔h; Gatsogiannis and Markl, 2009; Gatsogiannis et al., 2007; Markl, 2013; Zhang et al., 2013), resembling perfectly the association mode found in the crystal structures of FU-g from *Octopus dofleini* and the FU-h of KLH1, respectively (Cuff et al., 1998; Jaenicke et al., 2010, 2011). Like in the mega-hemocyanin complex from

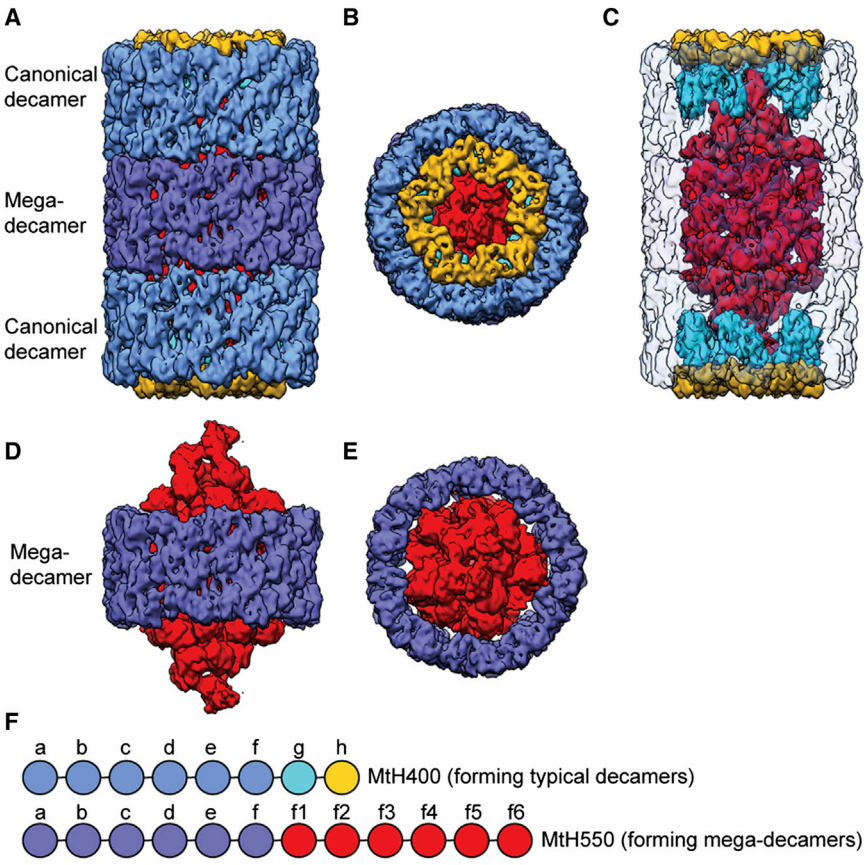

Figure 2. Structure of the MtH-hetero-30-mer
(A–C) Cryo-EM structure of the mega-tridecamer in side view (A), top view (B), and side view with the cylinder wall shown transparent (C) to reveal the inner rhombus and the peripheral collar complexes. Color code according to (F).
(D and E) Extracted density of the mega-decamer in side (D) and top view (E).
(F) Schematic representation of a typical gastropod hemocyanin subunit and MtH400 with eight distinct FUs (upper scheme) and the subunit of MtH550 with 12 different FUs (lower scheme).
See also Figures S1, S2, S4, and S5.

Leptoxis carinata (Lieb et al., 2010), the terminal FUs g and h form a collar at the opposing ends of the cylinder (Figures 2A–2C).

The architecture of the MtH550 mega-decamer, however, differs considerably from that of other hemocyanins. The overall symmetrical spinning top-like shape of the mega-decamer results from an inner stretched rhombus that is surrounded by an outer belt (Figures 2D and 2E). Whereas the latter one together with the two copies of MtH400 decamers forms the cylinder of MtH (Figure 2A), the rhombus fills the inner core of the MtH tridecamer (Figure 2C). Rigid-body fitting of homology models confirmed that the first six FUs of the ten subunits (a→f) form the belt, whereas the remaining six FUs (f1–f6) build the rhombus (Figures S3C–S3F). Interestingly, in agreement with our earlier hypothesis (Lieb et al., 2010), the D5 symmetrically organized segments of FUs a-b-c-d-e-f in the belt show the typical homodimeric antiparallel arrangement similar to the MtH400 decamers (Figures 3A–3C), suggesting a high overall structural conservation of molluscan hemocyanin cylinder walls. The antiparallel arrangement continues in the central rhombus with the two subunits contributing with their segments f1→f6 to opposing halves of the rhombus (Figures 3D–3H). Noteworthy, segments f1→f6 within such a dimer are found in specific combinations of conformations (Figures 3D–3H).

The organization of the inner rhombus is quite complex and differs from that of the cylinder. It is composed by two antiparallel arranged halves, resembling two jigsaw puzzle pieces, that dock to each other (Figures 4A and 4B). Compared to the linkers between the FUs of the cylinder wall, the connections between the FUs in the inner rhombus are shorter (1–7 versus 10–16 amino acids; Table S1). This prevents the FUs within the subunit segments f→f6 from forming heterodimers and almost fixes the connection between FUs f and f1 (Table S2). Despite this, the ten copies of segments f1→f6 of MtH550 are flexible enough to acquire five different conformations (conformer 1–5) equally positioned in the upper and lower part of the rhombus (Figures 3D–3H, 5A, and 5B; Movie S1). The conformers (not to be confused with isomers) differ considerably in their overall structure. Whereas conformers 1–3 are elongated (group I), conformers 4 and 5 adapt a more compact form (group II; Figures 3D–3H and 5B–5G; Movie S1).

Each half of the rhombus consists of an annulus with two tiers: the rhombus tip and a cube-like structure on the opposing side (Figures 4B, 4D, 4H, and 4L). At the point of transition between the cylinder wall and the rhombus (segment f-f1-f2), the five different conformers are almost identical (Figures 5C–5G; Table S2), forming the pseudo-5-fold symmetrical annulus (Figures 4D–4F). A hinge between f2 and f3 defines the overall orientation of the conformers (Figures 4C, 4G, and 5C–5G). Whereas the C′-termini of FUs f3 in the group I conformers point upward (Figures 4H–4J and 5C–5E), those of group II conformers are directed downward (Figures 4L–4N, 5F, and 5G). This arrangement allows for a complete filling of the annulus and presets the position of the remaining subunit segments (Figures 4K and 4O). Thus, the segments f4-f5-f6 of group I conformers form the tip of the rhombus (Figures 4H and 4K), whereas the respective segments of group II conformers form a compact complex laterally placed at the base of the half rhombus (Figures 4L and 4O). Certain flexibility between FU-f3 and FU-f4 and between FU-f5 and FU-f6 (Table S2) allows for an individual nonsymmetrical arrangement of each conformer, which results in a complete filling of the cylinder lumen (Figure S5).

Cryo-EM Structure of *Terebralia palustris* Mega-Hemocyanin

To find out if the complex arrangement of MtH is conserved in mega-hemocyanins of different cerithioid families or if it is

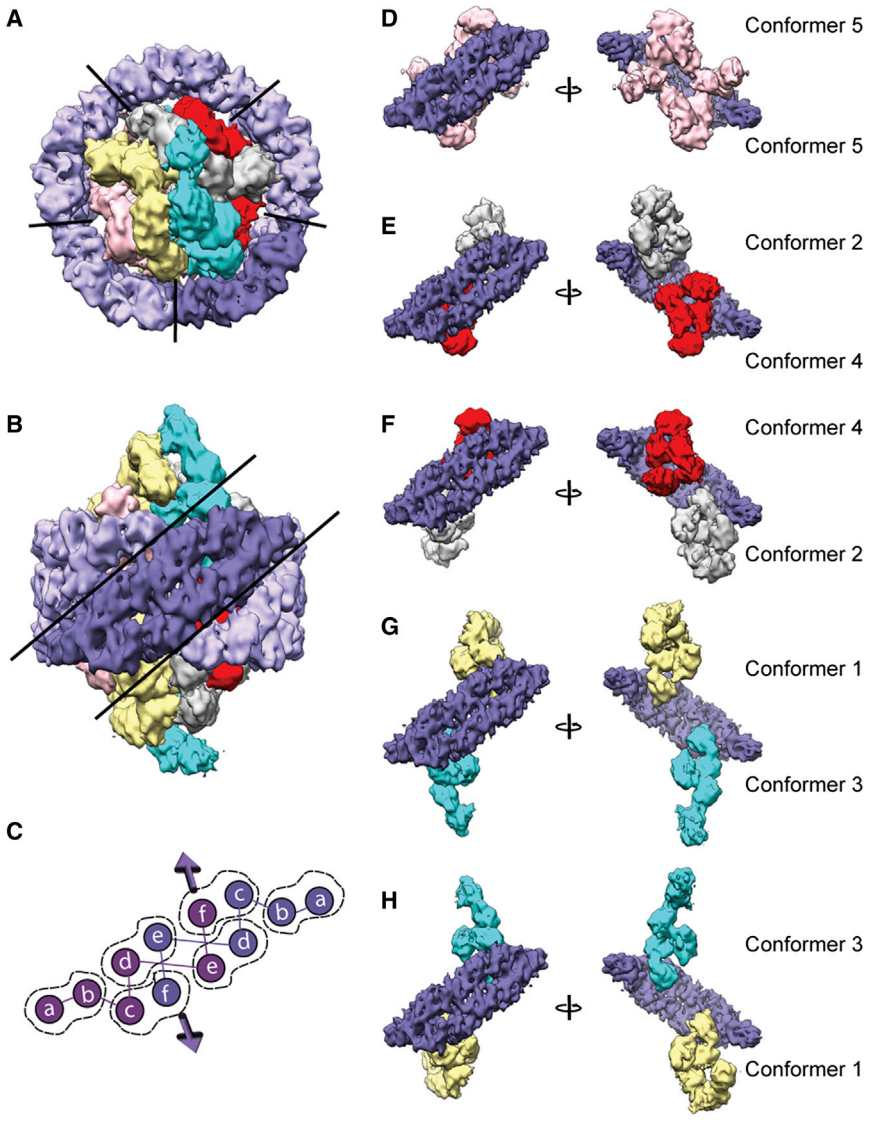

Figure 3. Architecture and Topology of the Five Subunit Dimers of the MtH Mega-Decamer

(A and B) Cryo-EM structure of the mega-decamer in top (A) and side (B) view. Cylinder wall shown in purple; the five different conformers of segment f1-f2-f3-f4-f5-f6 forming the inner rhombus complex are highlighted in color (conformer 1, yellow; conformer 2, gray; conformer 3, cyan [group I] and conformer 4, red; conformer 5, pink [group II]). The cylinder wall consists of five dimers of segment a-b-c-d-e-f, one of which is highlighted. Lines indicate borders between adjacent dimers.

(C) Scheme of the model in (B), depicting the topology of FUs a→f. FUs a/b, c/f, and d/e show a characteristic arrangement as morphological units, resembling the crystallographic dimers of *Octopus dofleini* hemocyanin FU-g (OdH-g) (PDB ID: 1JS8). Lines represent linker peptides connecting subsequent FUs. Arrows indicate how the pathway continues from the last FU of the wall (FU-f) to the first FU of the rhombus (FU-f1).

(D–H) Shown are two different side views of the five different putative dimers assembling the mega-decamer, after vertical rotation of 180°. According to the conformation of the two opposing segments f1-f2-f3-f4-f6 within each dimer, the resulting structure is a homo- (D) or a heterodimer (E–H).

more variable as suggested by the previously described variations of the collar complex in hemocyanins formed by seven to eight FUs (Gatsogiannis and Markl, 2009; Lamy et al., 1998; Markl, 2013), we used cryo-EM to analyze TpH, the mega-hemocyanin from a further cerithioid, *Terebralia palustris*, a mangrove snail from Kenya. In contrast to *M. tuberculata*, this animal is much larger, allowing collection of larger volumes of hemolymph, which makes it easier to obtain sufficient amounts of pure mega-tridecamers (Figure 6A). When reconstructing the structure of TpH, we found the same symmetry mismatch as for MtH. We therefore applied the same method as described above to obtain a cryo-EM reconstruction of the TpH tridecamer at an average resolution of 10.4 Å (Figure S2A). Again, the outer cylinder wall appears better resolved than the inner rhombus complex (Figure S2C). TpH shows in general all features present in the reconstruction of MtH (Figures 6B and 6C), but a careful comparison of the rhombus complexes revealed a major difference between the two complexes. The extracted central inner rhombus of TpH shows a less-compact architecture with additional fenestrations and a less-pointed rhombus tip (Figure 6D). The measured volume of the inner TpH rhombus appears to be 15%–20% less than that of the MtH rhombus. Superposition of both rhombi revealed that they are almost identical at this resolution, but the TpH structure misses ten densities (Figure 6E). These densities correspond mainly to the terminal FU-f6 of MtH and the adjacent C′-terminal β sandwich domain of FU-f5 (Figure 6F). This is also reflected in the difference map between the inner complexes of TpH and MtH (Figures 6G and 6H). In TpH, FU-f5 appears by far less well resolved, not only in comparison to FU-f5 of MtH but also to all other FU types. Although we chose the fit with the highest cross-correlation, the docking in this case is far less well reliable, suggesting a higher degree of flexibility for FU-f5 of TpH. Although we still lack the sequence of TpH, the present structural data clearly suggest that the central rhombus of TpH is composed of subunits with 11 instead of 12 FUs. But, apart from the missing terminal FU, TpH and MtH are equally built, suggesting a conserved structure of cerithioid mega-hemocyanins.

DISCUSSION

In the present study, we aimed to determine the structure of mega-hemocyanins from two species, namely *Terebralia palustris* (TpH) and *Melanoides tuberculata* (MtH), from two different families of the superfamily Cerithioidea to elucidate the complex

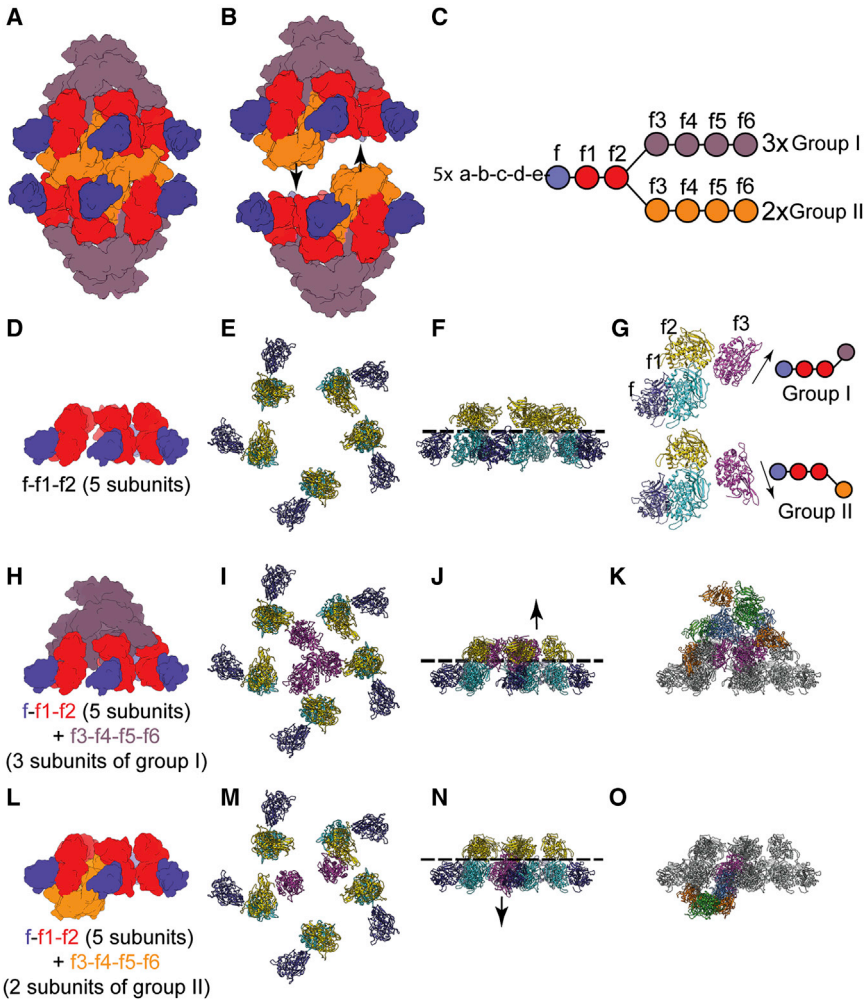

Figure 4. FU Arrangement within the Inner Rhombus Complex of MtH

(A and B) Extracted densities of the two opposing rhombus halves. Arrows indicate how they assemble to form the complete inner complex. FUs f and f1-f2 are depicted in blue and red, respectively. FUs f3→f6 are either shown in gray (group I) or orange (group II).

(C) Schematic representation of the five different conformer types that can be split in two groups. Color code according to (A).

(D) Side view of the annular structure formed by segments f-f1-f2 of the five different subunit conformers.

(E and F) Molecular model of (D) in top (E) and side view (F). FUs f, f1, and f2 shown in purple, cyan, and gold, respectively. Note the pseudo-5-fold symmetry in (E). Dashed line in (F) indicates the two tiers of the annulus.

(G) Molecular model of segment f-f1-f1-f3 in group I (upper image) and group II (lower image) conformers. Note the overall similarity of segment f-f1-f2 and direction change in FU-f3 (magenta), indicated by arrows and shown in the respective schemes.

(H) Side view of the annular structure shown in (D) together with segments f3-f4-f5-f6 of the three group I conformers, forming the rhombus tip.

(I and J) Molecular model of (D) together with three copies of FU-f3 stemming from the three group I conformers in top (I) and side view (J). Note that they fill the upper tier of the annulus (I and J).

(K) Molecular model of (H). FUs f4, f5, and f6 shown in blue, green, and brown, respectively.

(L) Side view of annular structure shown in (D) together with segments f3-f4-f5-f6 of the two group II conformers, forming a laterally placed cube-like structure.

(M and N) Molecular model of (D) together with two copies of FU-f3 stemming from the two group II conformers in top (M) and side (N) view. Note that they fill the lower tier of the annulus.

(O) Molecular model of (L).

See also Figure S3.

arrangement of their subunits. Mega-hemocyanins are composed of a central mega-decamer that is flanked by two normal decamers forming a hetero-30-mer (Lieb et al., 2010). The structures of TpH and MtH reveal a complex organization of the central mega-decamer. Different conformations of FU f1→f6 segments and their flexible arrangement result in a complete filling of the cylinder formed by the FUs a→f of the mega-decamer and the two flanking normal decamers. Although the overall arrangement of the subunits is the same in both species, TpH is missing the sixth (f6) C′-terminal FU in the central mega-decamer. The mega-decamer, although formed by ten identical subunits, shows a collection of local symmetries (including D5, C5, and C2) and is a rare case of a homo-oligomer showing several symmetry breaks. The symmetry mismatches do not stem from the different topological arrangement of identical homoprotomers, like for example in viruses, but from homoprotomers that take different conformations. Looking at these complex structures, two major questions arise: how do the ten subunits of the mega-decamer fold into such a mammoth structure in vivo, especially taking into account that the subunits are conformers and not isomers? And how did these convoluted mega-hemocyanins evolve?

Assembly of the Mega-Decamer

Reassembly experiments with isolated MtH subunits revealed that, depending on the buffer conditions, MtH550 readily self-assembles into mega-decamers, whereas MtH400 forms typical decamers, didecamers, and multidecamers (Lieb et al., 2010). This means that neither MtH400 nor chaperones are required for the formation of the central mega-decamer. Furthermore, because the MtH550 conformers are identical in sequence, the rhombus-like structure of the MtH core cannot be predetermined by preshaped conformers. The basic repeating unit of molluscan hemocyanins is the antiparallel subunit dimer, and it has been observed in many EM studies that the cylinder wall disassembles and reassembles stepwise by releasing, respectively adding, subunit dimers (for review, see van Holde et al., 2001 and Markl, 2013). It is tempting to speculate that this is also the case with the mega-decamer and the complete cylinder wall of the mega-decamer would form in a first assembly step. This would fix the ten

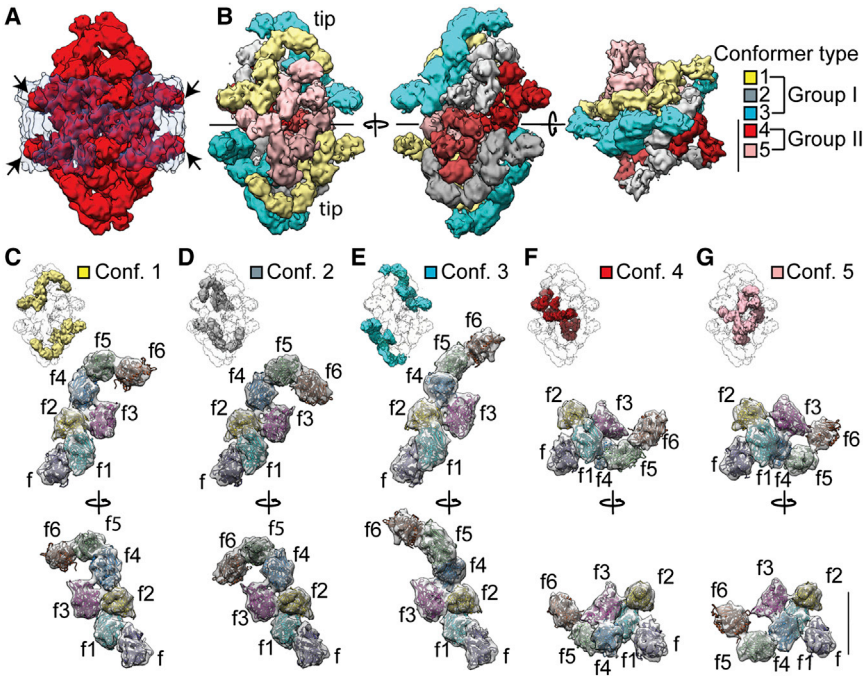

Figure 5. Architecture of the Inner Rhombus Complex of MtH

(A) Extracted density of ten copies of the segment f-f1-f2-f3-f4-f5-f6 (red). FUS f1→f6 form the rhombus complex, whereas FU-f (arrow) is the last FU of the cylinder wall, positioned in its upper and lower wall tier (transparent), each with five copies.

(B) Topology of the five different conformer types of MtH550 subunit within the rhombus complex. Shown are two different side views of the rhombus complex after vertical rotation of 180° around their longest axis and a top view. The five different conformations are depicted according to the color code in Figure 3.

(C–G) Shown are two side views of the extracted densities of the five conformers after vertical rotation of 180° with their respective homology models. Molecular models of FUs f, f1, f2, f3, f4, f5, and f6 are shown in purple, cyan, gold, magenta, blue, green, and brown, respectively. For each conformer, its topology within the rhombus is shown (upper image). The different conformers are categorized in two groups, based on the overall appearance: group I, which contains conformers 1 (C), 2 (D), and 3 (E), and group II, with conformers 4 (F) and 5 (G). All densities are extracted from the reconstruction of the MtH mega-tridecamer.

See also Figure S3 and Movie S1.

segments a-b-c-d-e-f, with the still wobbling segments f1-f2-f3-f4-f5-f6 protruding into the center. However, this is sterically not possible. Therefore, two scenarios are conceivable for the assembly of the mega-hemocyanin complex. Either the protomers assemble one after the other and the previous conformer determines the conformation of the following or the protomers come together at the same time with wobbling FUs simultaneously finding their position inside the rhombus. For both possibilities, a high flexibility of the protomers is an essential prerequisite for their origami-like arrangement. In this line, recent SAXS data showed that FUs of a molluscan hemocyanin can oscillate around their flexible linkers when not assembled (Spinozzi et al., 2012). However, at this stage, it is difficult to predict the mechanism of mega-hemocyanin assembly. If obtainable, structural analysis of partially disassembled or reassembled mega-hemocyanins would give further insights into how the complexes are formed in vivo.

Evolution of Mega-Hemocyanins

Based on previous sequence and structural data of various molluscan hemocyanins (for review, see Lieb and Markl, 2004; Markl, 2013; and Miller et al., 1998) and the present cryo-EM reconstructions of the two mega-hemocyanins, we present a model for the evolution of these fascinating oxygen transporters. The eight FU types that form the basic 400 kDa subunit evolved around 740 million years ago (Lieb et al., 2000; Lieb and Markl, 2004). Moreover, all molluscan hemocyanins analyzed so far are based on cylindrical decamers (Gatsogiannis and Markl, 2009; van Holde et al., 2001; Markl, 2013; Meissner et al., 2000; Zhang et al., 2013). We therefore assume that a decamer composed of eight-FU subunits is the archetypical complex from which other hemocyanins evolved, including the mega-hemocyanins of Cerithioidea, which appeared only 200 million years ago (Figure 7A). Another prerequisite for our evolutionary model is that, as in many other mollusks (Lieb and Markl, 2004), two isoforms of hemocyanin were available in evolutionary ancient Cerithioidea. Indeed, phylogenetic trees derived from the available FU sequences show that the segments a-b-c-d-e-f of MtH400 and MtH550, respectively, evolved by gene duplication of an ancestral eight-FU subunit (Markl, 2013). The presence of two hemocyanin isoforms is also known for various other gastropods, for example, *Megathura crenulata* and *Haliotis tuberculata* (Lieb and Markl, 2004; Markl, 2013).

This situation allowed a divergent evolution of both isoforms in the early Cerithioidea. Whereas one isoform remained unchanged, the other changed tremendously during evolution. We assume that one of the hemocyanin isoforms lost its two C′-terminal FUs during the early evolution of mega-hemocyanins. In fact, hemocyanins containing only subunits with seven or six FUs are found in living mollusks such as the cephalopods *Nautilus* and *Octopus* (Bergmann et al., 2006; Gatsogiannis et al., 2007; Meissner et al., 2007; Miller et al., 1998) and in the gastropod *Biomphalaria glabrata* (Lieb et al., 2006). They miss the terminal or the two terminal FUs, respectively (Figures 7B and 7C). In the case of *Biomphalaria glabrata* (family Planorbidae), hemocyanins with six-FU subunits form empty cylinders that miss the peripheral collar (Lieb et al., 2006; Figure 7C). Thus, even without the two terminal FU types, the formation of the cylinder wall is possible. The cylinder, which is formed by five symmetrical dimers of the antiparallel arranged segment a-b-c-d-e-f, represents the only structural complex that is found without variations throughout all molluscan hemocyanins characterized so far (Gatsogiannis and Markl, 2009; Gatsogiannis et al., 2007; Harris et al., 2004; Markl, 2013; Spinozzi et al., 2012; Zhang et al., 2013). Although the Planorbidae are not closely related to the Cerithioidea, the ‘‘truncated’’ hemocyanin

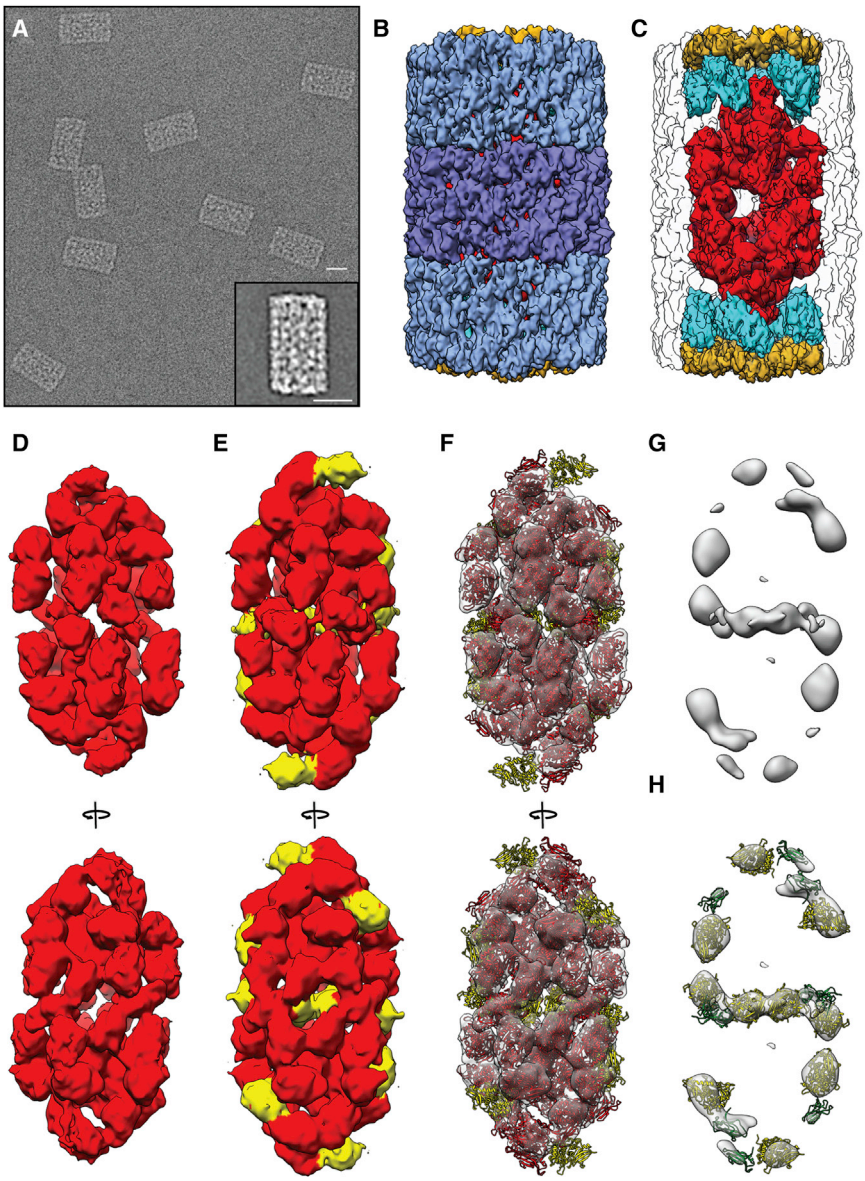

Figure 6. Cryo-EM Structure of TpH and Its Comparison to MtH

(A) Subarea of an unprocessed digital micrograph of purified TpH hetero-30-mers. Outlined box shows a characteristic class average of the TpH-hetero-30-mer. The scale bars represent 20 nm.

(B) Cryo-EM structure of TpH in side view. Color code as in Figure 2.

(C) Same as (B) but with the cylinder wall shown transparent to reveal the inner rhombus and the peripheral collar complexes.

(D) Extracted electron density of the rhombus complex of TpH shown in two different side views after vertical rotation of 180°.

(E) Extracted electron density of the rhombus complex of MtH shown in two different side views after vertical rotation of 180°. Additional densities in comparison to TpH are shown in yellow.

(F) Fitting of the molecular model of MtH into the extracted electron density of the rhombus complex of TpH. The ten copies of the terminal FU-f6 of MtH are colored yellow.

(G) Difference map between the rhombus complexes of TpH and MtH. Note the ten major and ten minor peaks.

(H) Topological comparison of the difference map shown in (G) with the molecular model of MtH. Shown are parts of the molecular model included within the densities of the difference map (FU-f6 shown in yellow and β sandwich domain of FU-f5 shown in green).

See also Figure S2.

of *B. glabrata* can serve as an initial state model toward the evolution of mega-hemocyanins. The additional five or six FUs (f1 → f5 and f1 → f6, respectively) that we identified in this study in the central mega-decamer of mega-hemocyanins were presumably added by repeated exon duplication events that, according to the phylogenetic tree (Markl, 2013), started from FU-f (Figures 7D–7G). Gene duplications have also been described for hemocyanins from *Sepia* (Lamy et al., 1998). In this case, however, one of the internal instead of the terminal FUs was duplicated.

Based on our reconstructions of the two mega-hemocyanins, we propose the following evolutionary steps for the sequential addition of subunits: starting from a six-FU subunit, the two first duplicated copies of FU-f (f1-f2) followed the antiparallel arrangement of the wall segments within the decamer, resulting in protrusions into the lumen of the cylinder (Figure 7D). The linkers within the segments f-f1-f2 are shorter than those within the segments f-g-h of the archetypical decamer (Table S1). This results in the formation of two annuli instead of a collar-like structure as observed in the flanking decamers (Figure 7D). The space inside the cylinder is not yet restricted at this stage, and therefore the FUs of the annuli are not forced to break the symmetry. Thus, each annulus that is formed by segment f1-f2 is C5 symmetrical, resulting in an overall D5 symmetry. The gain of an additional FU (f3) resulted in the first symmetry break (Figure 7E). Because the collar of the flanking decamers sterically hinders addition of subunits in the upward or downward direction, three copies of FU-f3 continue pointing to the center of the lumen. However, the space for the remaining two FU-f3 copies is restricted by the diameter of the annulus, so they have to be oriented differently. The three first copies are then positioned in the outer tier of the annulus whereas the remaining two copies are positioned in the inner tier (Figure 7E). This breaks the 5-fold symmetry. The resulting bend in the pathway of the subunits is made possible by the architecture of the hemocyanin subunit. It resembles a ''pearl necklace'' of FUs interconnected by flexible linker peptides with the FUs wobbling around their linker peptides when not assembled (Spinozzi et al., 2012). The next two FUs (f4-f5) then almost completely fill the remaining space between the central annulus and the flanking decamers by taking different conformations (Figures 7F and 7H). This gives the core of the

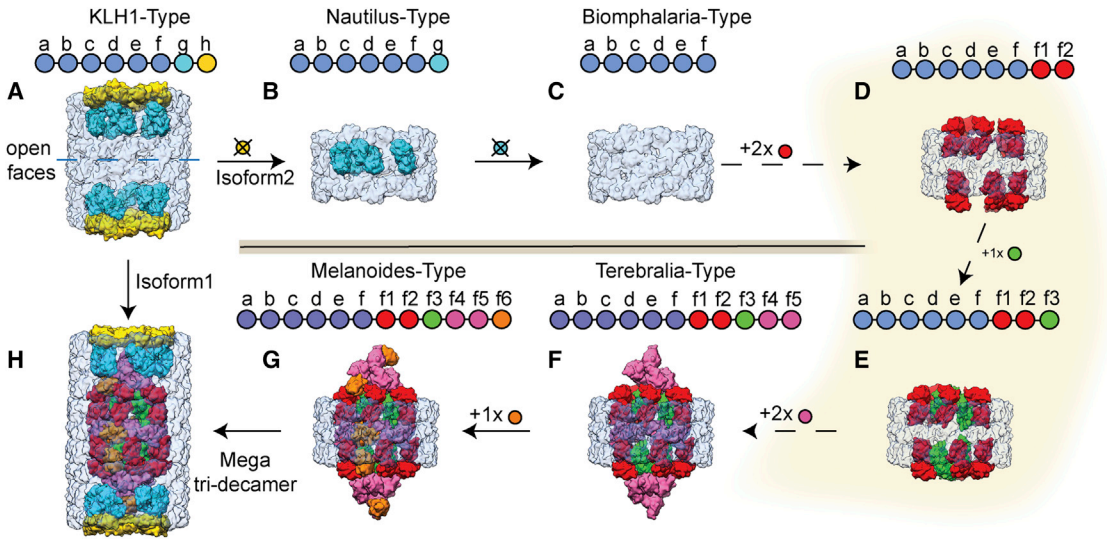

Figure 7. Model for the Evolution of Mega-Hemocyanins

(A) The hypothetical phylogenetic origin of mega-hemocyanins is probably a didecamer composed of protomers with eight FUs (Markl, 2013). Similar to the typical gastropod hemocyanin didecamers (e.g., KLH), they must have existed in two isoforms in the same animal. Whereas the FUs a–f form a cylindrical wall, the FUs g and h build an asymmetrically arranged collar. Two decamers assemble at their open sides to form a didecamer.

(B) Whereas one of the isoforms remained unchanged during evolution, the second lost the terminal FU-h, together with the ability to form homodidecamers. The resulting decamer must have resembled the typical hemocyanin of *Octopus* and *Nautilus*, with only a single FU (FU-g) building the asymmetric collar complex.

(C) After further loss of the terminal FU-g, the resulting hemocyanins have probably been similar to those found in the hemolymph of *Biomphalaria glabrata*.

(D) Subsequent addition of two FUs (f1 and f2) by duplication of the terminal FU-f added an annular structure at each face of the decamer. The orientation of these FUs differs from their arrangement in KLH1 (A).

(E) Addition of another FU (f3) filled each annulus in its center. Because of steric hindrance, three of the FU-f3s point upward and the remaining two downward.

(F and G) Additional gain of further FUs resulted in an asymmetric enlargement of the annulus at both sides. The mega-decamers of TpH and MtH have two and three additional FUs after FU-f3, respectively.

(H) Two decamers of the second isoform dock at each side of the mega-decamer of the first isoform, forming thereby a large 13.5 MDa mega-hemocyanin. The protruding masses of the growing rhombus prohibited homodimerization of mega-decamers. But the clear-shape complementarity between the rhombus and the inner lumen formed by the collars and walls of the hetero-30-mer suggest that complex formation with typical decamers of the second isoform was probably the case during evolution. At all stages, the FUs of the rhombus had to fit into the lumen of the mega-tridecamer.

Steps in evolution highlighted in color represent hypothetical protein complexes. All other protein complexes shown represent hemocyanins that are found in living animals. Color code according to Figure 2.

mega-hemocyanin its rhombus-like appearance and represents the situation in TpH. However, the central rhombus in this case is not rigid but shows several local flexibilities. Addition of a further FU (f6) as in MtH results then in a complete packing of the space inside the flanking decamers and, due to additional interfaces, stabilizes the entire inner rhombus (Figures 7G and 7H). Although a fully packed mega-tridecamer occupies the same space in the hemolymph as a typical gastropod hemocyanin tridecamer, it contains 40 additional oxygen-binding sites that render mega-hemocyanins more efficient, without increasing hemolymph viscosity or colloid-osmotic pressure. Other mollusks are also capable to form stacked multidecamers of varying length. However, the mobility of such large elongated complexes might be reduced inside the hemolymph. With respect to oxygen binding, mega-hemocyanins show a higher degree of functional plasticity and higher oxygen affinities than typical molluscan hemocyanins. This seems to allow these animals to survive under hypoxic conditions (Lieb et al., 2010). Therefore, living in these environments was probably the main selection pressure that acted on the hemocyanin genes, resulting in the highly efficient mega-hemocyanins. An alternative strategy was dismissal of hemocyanin and expression of hemoglobin with high oxygen affinity instead as in the case of planorbid snails (Lieb et al., 2006).

To further identify missing links, it might be worthwhile to scan other cerithioid mega-hemocyanins for subunits with less than 11 FUs. Identification of such hemocyanins, if they exist, would support our model and enable to trace the evolution more accurately from a structural point of view.

Noteworthy, according to the present model, the decamer appears not only as the main assembly intermediate but also as the main evolutionary unit. This further supports the idea that, among proteins, an intermediate in the assembly of a complex also represents a form in its evolutionary pathway (Levy et al., 2008).

Additional Interfaces Stabilize the Complex

The origami-like arrangement of FUs within the rhombus results in additional interfaces in mega-hemocyanins. Basically every FU of the internal rhombus interacts differently with its direct and more-distant neighbors compared to the situation in the more-simple archetypical decamer. This leads to a stabilization of the mega-decamer. However, because the contact regions vary strongly, this effect must rather result from nonspecific interactions than

from specific ones. Interestingly, the affinity of the flanking decamers for interacting with each other is much lower than forming a mega-hemocyanin by interacting with a mega-decamer (Lieb et al., 2010). Thus, the arrangement of the FUs in the rhombus not only causes the stabilization of the rhombus itself but also create additional stabilizing interfaces with the collar and cylinder of the flanking decamers. This is probably an important prerequisite for a stable mega-hemocyanin complex formation. In the future, structures at atomistic resolution will allow studying the nature of these interfaces in more detail.

Conclusions

This striking example of protein origami demonstrates that a complex structure can be built by using a single "pearl necklace"-like polypeptide as building block. The present structures of two of these fascinating mega-hemocyanin complexes raise the question of how they fold and assemble and give insights into how they might have evolved. Understanding the mechanism of building such a large functional protein complex could be interesting for synthetic biology approaches and could be used as a blueprint for engineering other protein complexes using flexible building blocks.

EXPERIMENTAL PROCEDURES

Animals and Hemocyanin Preparation

Hemolymph was taken from *Terebralia palustris* (Gastropoda; Potamidae) and *Melanoides tuberculata* (Gastropoda; Thiaridae) and purified as described previously (Lieb et al., 2010). Purified hemocyanin was stored at 4°C in "stabilizing buffer" (50 mM Tris/HCl [pH 7.4], 150 mM NaCl, 5 mM $CaCl_2$, and 5 mM $MgCl_2$).

Electron Cryomicroscopy

TpH and MtH were applied to holey carbon grids (C-flats; protochips) with a thin layer of continuous carbon and vitrified using a CryoPlunge3 (Cp3; Gatan). Images were taken with a JEOL JEM 3200 FSC electron microscope equipped with a field emission gun at an operation voltage of 200 kV, at a defocus range of 0.4–2.4 μm. An omega in-column energy filter was used with a slit width of 15 eV. The images were recorded with an 8k × 8k CMOS camera F816 (TVIPS) at a pixel size of 0.91 Å/pixel for MtH and 1.25 Å/pixel for TpH using minimal-dose conditions. The images were taken manually and automatically using the EMTools software package (TVIPS).

Image Processing

Defocus and astigmatism for each image were determined using in-house-developed software (C.G. and R. Efremov, unpublished data). Images with astigmatism and/or drift were discarded. For analysis of MtH, 24,188 single particles were selected manually from 652 digital micrographs using boxer from the EMAN software package (Ludtke et al., 1999).

Subsequent steps of image processing were performed with the SPARX software package (Hohn et al., 2007). Single particles were aligned and classified using reference-free alignment and k-means classification procedures as well as the iterative stable alignment and clustering approach (Yang et al., 2012). We then extracted 6,764 single particles from high-quality 2D class averages representing exclusively side views of complete mega-tridecamers (Figure 1B). After further classification, an initial model of MtH was created by the ab initio projection-matching approach implemented in SPARX using a featureless cylinder as starting reference, class averages, and C5 symmetry. Further projection-matching rounds were performed using a local symmetrization approach as previously described (Gatsogiannis et al., 2013; Meusch et al., 2014). Briefly, after removal of the inner collar complex, the resulting 3D volume of the cylinder wall was used as starting reference for projection matching with no imposed symmetry. After each refinement round, we extracted the densities corresponding to the cylinder wall and inner collar complex and symmetrized them with D5 and D1 symmetry, respectively. We used "D1" symmetry because the 2-fold symmetry axis of the rhombus runs perpendicular to the 5-fold symmetry axis of the cylinder wall. The threshold of both densities was then scaled, and subsequently, the two densities were combined to one. The resulting volume was further masked to remove background noise and used as reference for the next refinement round. Using the same approach, a reconstruction of TpH was created from 30,527 single particles from 1,636 digital micrographs. The average resolution of both reconstructions was determined by using the FSC 0.5 criterion. Local resolution calculations were performed as described previously (Anger et al., 2013) using a 20 Å sphere for windowed FSC calculations at 0.5.

Homology Modeling, Rigid-Body Fitting, and Visualization

Sequences of the 12 different FUs of MtMH550 and eight different FUs of MtH400 are available (GeneBank entries KC405575 and KC405576) and show high conservation of areas corresponding to secondary structures elements of the crystal structures of *Megathura crenulata* hemocyanin FU-h (KLH1-h) (Protein Data Bank [PDB] ID: 3QJO), *Octopus dofleini* hemocyanin FU-g (OdH-g) (PDB ID: 1JS8), and *Rapana thomasiana* hemocyanin FU-e (PDB ID: 1LNL). This allowed molecular modeling of the respective FUs using MODELLER (Eswar et al., 2008).

The obtained homology models for the eight FU types of MtH400 and FU-a to FU-f of MtH550 were then subsequently rigid-body fitted into the density map of MtH, according to the topology previously described for gastropod hemocyanins (Gatsogiannis and Markl, 2009; Zhang et al., 2013). To elucidate the structure of the inner-rhombus-like complex of MtH, we first automatically rigid-body fitted 60 copies of the crystal structure of OdH-g (PDB ID: 1JS8), which is the prototype of a typical 50 kDa FU type. To reveal the topology of the different FUs within the inner complex, we analyzed based on these preliminary fittings how the polypeptide chain continues from FU-f of the wall to f1 → f2 → f3 → f4 → f5 → f6. Due to the lower symmetry, this analysis was performed for all ten copies of the 550 kDa subunit. In comparison to other molluscan hemocyanins, the linker peptides connecting f1 → f2 → f3 → f4 → f5 → f6 encompass only 1–7 amino acids (Table S1) and this feature simplified the topological analysis and left in each case only a single possibility how the subunit pathway continues from the last secondary structure of the preceding FU (strand β13) to the first secondary structure of the subsequent FU (strand β1).

Based on this topological analysis, each of the 60 docked copies of OdH-g was replaced with the homology model for the respective FU. Fitting of the homology models of the different FUs into their respective positions within the density map of MtH was done using Chimera (Pettersen et al., 2004). Detailed analysis of the different conformers of MtH500 and identification of hinge axes and bending residues (Table S2) was performed with the DynDom Server (Lee et al., 2003). Fitting-based segmentation of the map was done with the tool "color zone" of Chimera. Morphing between the different conformers was calculated using the tool "Morph Conformations" in Chimera and recorded as a movie (Movie S1). For visualization, analysis, and preparation of figures, we also used Chimera. All EM densities were filtered to their average resolutions.

ACCESSION NUMBERS

The coordinates for the EM structures of MtH and TpH have been deposited in the EM Data Bank under accession codes EMD-6185 and EMD-6186, respectively.

SUPPLEMENTAL INFORMATION

Supplemental Information includes five figures, two tables, and one movie and can be found with this article online at http://dx.doi.org/10.1016/j.str.2014.10.013.

AUTHOR CONTRIBUTIONS

C.G. screened samples. C.G. and O.H. collected EM data; C.G. processed, refined, and analyzed EM data; C.G. and S.R. wrote the paper; J.M. cowrote

the paper; and C.G., J.M., and S.R. designed the study. All authors discussed and approved the results.

ACKNOWLEDGMENTS

We are grateful to R.S. Goody for continuous support. We thank E. Schubert for initial contributions, M. Neufurth and B. Lieb for providing us MtH sequences, and W. Gebauer for extracting the hemolymph and purifying the hemocyanin. *T. palustris* hemolymph was a gift of N. Hellmann. This work was supported by the "Deutsche Forschungsgemeinschaft" grant RA 1781/1-1 (to S.R.) and the Max Planck Society (to S.R.).

Received: July 1, 2014
Revised: September 22, 2014
Accepted: October 7, 2014
Published: December 4, 2014

REFERENCES

Anger, A.M., Armache, J.-P., Berninghausen, O., Habeck, M., Subklewe, M., Wilson, D.N., and Beckmann, R. (2013). Structures of the human and Drosophila 80S ribosome. Nature *497*, 80–85.

Becker, M.I., Arancibia, S., Salazar, F., Del Campo, M., and De Ioannes, A. (2014). Mollusk hemocyanins as natural immunostimulants in biomedical applications. In Immune Response Activation, H.T. Duc (InTech). http://www.intechopen.com/books/immune-response-activation/mollusk-hemocyanins-as-natural-immunostimulants-in-biomedical-applications.

Bergmann, S., Lieb, B., Ruth, P., and Markl, J. (2006). The hemocyanin from a living fossil, the cephalopod Nautilus pompilius: protein structure, gene organization, and evolution. J. Mol. Evol. *62*, 362–374.

Beuron, F., Maurizi, M.R., Belnap, D.M., Kocsis, E., Booy, F.P., Kessel, M., and Steven, A.C. (1998). At sixes and sevens: characterization of the symmetry mismatch of the ClpAP chaperone-assisted protease. J. Struct. Biol. *123*, 248–259.

Cuff, M.E., Miller, K.I., van Holde, K.E., and Hendrickson, W.A. (1998). Crystal structure of a functional unit from Octopus hemocyanin. J. Mol. Biol. *278*, 855–870.

Decker, H., Hellmann, N., Jaenicke, E., Lieb, B., Meissner, U., and Markl, J. (2007). Minireview: Recent progress in hemocyanin research. Integr. Comp. Biol. *47*, 631–644.

Eswar, N., Eramian, D., Webb, B., Shen, M.Y., and Sali, A. (2008). Protein structure modeling with MODELLER. Methods Mol. Biol. *426*, 145–159.

Gatsogiannis, C., and Markl, J. (2009). Keyhole limpet hemocyanin: 9-A CryoEM structure and molecular model of the KLH1 didecamer reveal the interfaces and intricate topology of the 160 functional units. J. Mol. Biol. *385*, 963–983.

Gatsogiannis, C., Moeller, A., Depoix, F., Meissner, U., and Markl, J. (2007). Nautilus pompilius hemocyanin: 9 A cryo-EM structure and molecular model reveal the subunit pathway and the interfaces between the 70 functional units. J. Mol. Biol. *374*, 465–486.

Gatsogiannis, C., Lang, A.E., Meusch, D., Pfaumann, V., Hofnagel, O., Benz, R., Aktories, K., and Raunser, S. (2013). A syringe-like injection mechanism in Photorhabdus luminescens toxins. Nature *495*, 520–523.

Harris, J.R., and Markl, J. (1999). Keyhole limpet hemocyanin (KLH): a biomedical review. Micron *30*, 597–623.

Harris, J.R., and Markl, J. (2000). Keyhole limpet hemocyanin: molecular structure of a potent marine immunoactivator. A review. Eur. Urol. *37* (*Suppl 3*), 24–33.

Harris, J.R., Meissner, U., Gebauer, W., and Markl, J. (2004). 3D reconstruction of the hemocyanin subunit dimer from the chiton Acanthochiton fascicularis. Micron *35*, 23–26.

Hohn, M., Tang, G., Goodyear, G., Baldwin, P.R., Huang, Z., Penczek, P.A., Yang, C., Glaeser, R.M., Adams, P.D., and Ludtke, S.J. (2007). SPARX, a new environment for Cryo-EM image processing. J. Struct. Biol. *157*, 47–55.

Jaenicke, E., Büchler, K., Markl, J., Decker, H., and Barends, T.R.M. (2010). Cupredoxin-like domains in haemocyanins. Biochem. J. *426*, 373–378.

Jaenicke, E., Büchler, K., Decker, H., Markl, J., and Schröder, G.F. (2011). The refined structure of functional unit h of keyhole limpet hemocyanin (KLH1-h) reveals disulfide bridges. IUBMB Life *63*, 183–187.

Kurokawa, T., Wuhrer, M., Lochnit, G., Geyer, H., Markl, J., and Geyer, R. (2002). Hemocyanin from the keyhole limpet Megathura crenulata (KLH) carries a novel type of N-glycans with Gal(β1-6)Man-motifs. Eur. J. Biochem. *269*, 5459–5473.

Lamy, J., You, V., Taveau, J.C., Boisset, N., and Lamy, J.N. (1998). Intramolecular localization of the functional units of Sepia officinalis hemocyanin by immunoelectron microscopy. J. Mol. Biol. *284*, 1051–1074.

Lander, G.C., Estrin, E., Matyskiela, M.E., Bashore, C., Nogales, E., and Martin, A. (2012). Complete subunit architecture of the proteasome regulatory particle. Nature *482*, 186–191.

Lasker, K., Förster, F., Bohn, S., Walzthoeni, T., Villa, E., Unverdorben, P., Beck, F., Aebersold, R., Sali, A., and Baumeister, W. (2012). Molecular architecture of the 26S proteasome holocomplex determined by an integrative approach. Proc. Natl. Acad. Sci. USA *109*, 1380–1387.

Lee, R.A., Razaz, M., and Hayward, S. (2003). The DynDom database of protein domain motions. Bioinformatics *19*, 1290–1291.

Levy, E.D., Boeri Erba, E., Robinson, C.V., and Teichmann, S.A. (2008). Assembly reflects evolution of protein complexes. Nature *453*, 1262–1265.

Lieb, B., and Markl, J. (2004). Evolution of molluscan hemocyanins as deduced from DNA sequencing. Micron *35*, 117–119.

Lieb, B., Altenhein, B., and Markl, J. (2000). The sequence of a gastropod hemocyanin (HtH1 from Haliotis tuberculata). J. Biol. Chem. *275*, 5675–5681.

Lieb, B., Altenhein, B., Markl, J., Vincent, A., van Olden, E., van Holde, K.E., and Miller, K.I. (2001). Structures of two molluscan hemocyanin genes: significance for gene evolution. Proc. Natl. Acad. Sci. USA *98*, 4546–4551.

Lieb, B., Boisguérin, V., Gebauer, W., and Markl, J. (2004). cDNA sequence, protein structure, and evolution of the single hemocyanin from Aplysia californica, an opisthobranch gastropod. J. Mol. Evol. *59*, 536–545.

Lieb, B., Dimitrova, K., Kang, H.S., Braun, S., Gebauer, W., Martin, A., Hanelt, B., Saenz, S.A., Adema, C.M., and Markl, J. (2006). Red blood with blue-blood ancestry: intriguing structure of a snail hemoglobin. Proc. Natl. Acad. Sci. USA *103*, 12011–12016.

Lieb, B., Gebauer, W., Gatsogiannis, C., Depoix, F., Hellmann, N., Harasewych, M.G., Strong, E.E., and Markl, J. (2010). Molluscan mega-hemocyanin: an ancient oxygen carrier tuned by a ~550 kDa polypeptide. Front. Zool. *7*, 14.

Ludtke, S.J., Baldwin, P.R., and Chiu, W. (1999). EMAN: semiautomated software for high-resolution single-particle reconstructions. J. Struct. Biol. *128*, 82–97.

Markl, J. (2013). Evolution of molluscan hemocyanin structures. Biochim. Biophys. Acta *1834*, 1840–1852.

Marles-Wright, J., Grant, T., Delumeau, O., van Duinen, G., Firbank, S.J., Lewis, P.J., Murray, J.W., Newman, J.A., Quin, M.B., Race, P.R., et al. (2008). Molecular architecture of the "stressosome," a signal integration and transduction hub. Science *322*, 92–96.

Meissner, U., Dube, P., Harris, J.R., Stark, H., and Markl, J. (2000). Structure of a molluscan hemocyanin didecamer (HtH1 from Haliotis tuberculata) at 12 A resolution by cryoelectron microscopy. J. Mol. Biol. *298*, 21–34.

Meissner, U., Gatsogiannis, C., Moeller, A., Depoix, F., Harris, J.R., and Markl, J. (2007). Comparative 11A structure of two molluscan hemocyanins from 3D cryo-electron microscopy. Micron *38*, 754–765.

Meusch, D., Gatsogiannis, C., Efremov, R.G., Lang, A.E., Hofnagel, O., Vetter, I.R., Aktories, K., and Raunser, S. (2014). Mechanism of Tc toxin action revealed in molecular detail. Nature *508*, 61–65.

Miller, K.I., Cuff, M.E., Lang, W.F., Varga-Weisz, P., Field, K.G., and van Holde, K.E. (1998). Sequence of the Octopus dofleini hemocyanin subunit: structural and evolutionary implications. J. Mol. Biol. *278*, 827–842.

Morse, M.P., Meyhöfer, E., Otto, J.J., and Kuzirian, A.M. (1986). Hemocyanin respiratory pigment in bivalve mollusks. Science *231*, 1302–1304.

Perbandt, M., Guthöhrlein, E.W., Rypniewski, W., Idakieva, K., Stoeva, S., Voelter, W., Genov, N., and Betzel, C. (2003). The structure of a functional unit from the wall of a gastropod hemocyanin offers a possible mechanism for cooperativity. Biochemistry *42*, 6341–6346.

Pettersen, E.F., Goddard, T.D., Huang, C.C., Couch, G.S., Greenblatt, D.M., Meng, E.C., and Ferrin, T.E. (2004). UCSF Chimera—a visualization system for exploratory research and analysis. J. Comput. Chem. *25*, 1605–1612.

Slovin, S.F., Keding, S.J., and Ragupathi, G. (2005). Carbohydrate vaccines as immunotherapy for cancer. Immunol. Cell Biol. *83*, 418–428.

Spinozzi, F., Mariani, P., Mičetić, I., Ferrero, C., Pontoni, D., and Beltramini, M. (2012). Quaternary structure heterogeneity of oligomeric proteins: a SAXS and SANS study of the dissociation products of Octopus vulgaris hemocyanin. PLoS ONE *7*, e49644.

van Holde, K.E., Miller, K.I., and Decker, H. (2001). Hemocyanins and invertebrate evolution. J. Biol. Chem. *276*, 15563–15566.

Velkova, L., Dolashka, P., Lieb, B., Dolashki, A., Voelter, W., Van Beeumen, J., and Devreese, B. (2011). Glycan structures of the structural subunit (HtH1) of Haliotis tuberculata hemocyanin. Glycoconj. J. *28*, 385–395.

Wolf, M., Garcea, R.L., Grigorieff, N., and Harrison, S.C. (2010). Subunit interactions in bovine papillomavirus. Proc. Natl. Acad. Sci. USA *107*, 6298–6303.

Yang, Z., Fang, J., Chittuluru, J., Asturias, F.J., and Penczek, P.A. (2012). Iterative stable alignment and clustering of 2D transmission electron microscope images. Structure *20*, 237–247.

Zhang, Q., Dai, X., Cong, Y., Zhang, J., Chen, D.-H., Dougherty, M.T., Wang, J., Ludtke, S.J., Schmid, M.F., and Chiu, W. (2013). Cryo-EM structure of a molluscan hemocyanin suggests its allosteric mechanism. Structure *21*, 604–613.